

# Cosmic Ray Detectors: Principles of Operation and a Brief Overview of (Mostly) U.S. Flight Instruments

---

Cary Zeitlin, Ph.D.  
Principal Scientist  
Space Technologies  
Southwest Research Institute  
1050 Walnut St, Suite 300  
Boulder, CO 80302  
[zeitlin@swri.boulder.edu](mailto:zeitlin@swri.boulder.edu)

1

Reviewed

Posted to THREE April 30, 2012

# Cosmic Ray Detectors: Principles of Operation and a Brief Overview of (Mostly) U.S. Flight Instruments

## Contents

Introduction.....	3
The Physics of Charged Particle Detection .....	4
Basic Principles.....	4
Curvature in Magnetic Fields .....	6
Čerenkov radiation.....	7
Transition radiation.....	7
Observables.....	7
Charged Particle Detector Types .....	9
Organic Scintillators .....	9
Inorganic Scintillators.....	10
Track Detectors and TLDs.....	11
Tissue-Equivalent Proportional Counters.....	12
Silicon Detectors.....	12
Čerenkov Radiation Detectors.....	13
Ground-Based Air Shower Detectors .....	14
Calibration .....	14
Neutron Detection.....	14
A Brief Tour of Cosmic Ray Detectors .....	15
GOES.....	16
ACE/CRIS .....	16
HEAO-3-C2.....	17
MARIE.....	17
CRaTER.....	18
RAD for the MSL Mission .....	19
RAD for the ISS.....	21
Other Instruments .....	22
Conclusions and Acknowledgments.....	22
References.....	23

## Introduction

This article gives an overview of cosmic ray detectors, a vast subject, and for the sake of brevity many important topics must be skipped or only touched on lightly. A great deal of relevant material, including the fascinating history of particle detectors, is freely available online. Wikipedia in particular has many good articles, several of which are referenced here.

Among the earliest particle detectors were electrometers developed by Victor Hess, which he placed on balloons starting in 1912, to measure ionization as a function of altitude [1]. These measurements led to the realization that the top of the Earth's atmosphere is constantly bombarded by energetic particles. Measurements of space radiation in one form or another have been ongoing ever since. As our understanding of the nature of fundamental particles and their interactions has grown, so too have the capabilities of particle detectors, in a synergistic cycle of experimental and theoretical advances. Particles arriving from space have always played an important role in basic physics, from Hess's measurements through the balloon-borne emulsion experiments that measured energetic heavy ions in space in the late 1940's [2], to the discovery of the van Allen belts in 1958 [3], to current searches for rare, ultra-high energy cosmic rays that are measured by reconstructing air showers of secondary particles [4]. To narrow the focus in this vast subject area, we will confine the discussion to detectors that are currently (or soon to be) in use and those that have made major contributions to our knowledge of space radiation in the last 30 or so years. Before discussing detectors, some basic concepts of particle detection are explained.

The particles that contribute to the health risks of extraterrestrial environments are not necessarily the same types or energies as those studied in heliospheric physics, magnetospheric physics, or planetary science. Nor are they the same types of particles that produce cosmic radiation at the surface of the Earth, since all particles impinging on the top of the atmosphere interact or stop at high altitudes. Rather, when considering space radiation and its effects on humans, we are concerned with energetic charged particles and neutrons in specific energy ranges. At the low end of the energy scale, the charged particles of interest are those with ranges greater than that of the minimum shielding employed, which is the thinnest parts of an astronaut's spacesuit worn during extra-vehicular activities (EVA); these parts present about  $0.2 \text{ g cm}^{-2}$  of areal density (equivalent to 2 mm of water) to incident particles [5]. While this depth of shielding has no effect on high-energy particles, it is sufficient to stop protons with kinetic energies below about 15 MeV or electrons below about 600 keV. There is no upper limit on the energies of interest, though in practical terms fluxes of Galactic Cosmic Rays (GCR) are not significant for dosimetric purposes above about 10 GeV/nucleon. Thus for present purposes, the vast quantity of data that has been obtained at energies lower or higher than the thresholds defined here – and the instruments used to obtain those data – are not of much interest. Because

neutrons with energies above a few hundred keV can make a significant contribution to the dose equivalent in shielded environments [6], we will also briefly discuss neutron detection.

To fully characterize various radiation environments, it is not sufficient to simply measure the Linear Energy Transfer (LET) spectrum at a particular point. The charge and energy distributions of the incident particles are also needed. (We refer throughout to LET, by which we mean the LET in an infinite volume of water, or  $LET_{\infty}$ .) These distributions are not static: they vary in time due to variations in the flux of Galactic Cosmic Rays – on the time scale of years – and due to sporadic Solar Particle Events with time scales of hours or days.

## The Physics of Charged Particle Detection

### Basic Principles

Charged particle detectors range in size and complexity from pieces of plastic that easily fit in the palm of one's hand (Plastic Nuclear Track Detectors [7] and thermoluminescent dosimeters [8]) to gigantic systems weighing hundreds of tons and with millions of channels of electronics that are used at CERN and other high-energy physics labs [9]. The mass, volume, power consumption, and complexity of a detector grow rapidly as functions of the particle energies that must be measured and the level of detail that must be extracted from the data. Though detector systems vary widely in size and complexity, the number of physical processes upon which most practical detectors are based is small: ionization energy loss, curvature of trajectories in magnetic fields, Cerenkov radiation, and transition radiation. For present purposes, the most important of these is ionization energy loss, which when measured accurately can tell us a great deal about a particle. Ionization energy loss per unit track length, or  $dE/dx$ , is accurately described by the Bethe-Bloch equation [10]. For ions, the equation can be written in units of MeV/cm as:

$$\frac{dE}{dx} = -0.30708\rho \frac{Z_m}{A_m} \frac{Z^2}{\beta^2} \ln\left(\frac{2m_e c^2 \beta^2}{I(1-\beta^2)} - \beta^2 - \delta - \frac{C}{Z_m}\right)$$

where  $Z$  is the charge of the particle,  $\beta$  is its velocity divided by  $c$  (the speed of light in vacuum),  $m_e$  is the electron mass,  $\rho$  is the density of the material being traversed in units of  $\text{g cm}^{-3}$ ,  $Z_m$  is atomic number of the material being traversed,  $A_m$  is its mass number, and  $I$  is its ionization potential. The terms  $\delta$  and  $C$  refer to the density effect and shell correction, respectively. The properties of the material being traversed are known, so measurements of  $dE/dx$  (or, to be more formally correct,  $\Delta E/\Delta x$  in a finite detector depth) can in principle directly reveal the charge and velocity of a given particle. However, most often a single measurement is ambiguous, for reasons explained below.

The shell correction is important only at low energies; the density effect is important at high energies, above several hundred MeV/nuc. An additional complication arises when one considers the “restricted” energy loss, which excludes the highest-energy so-called knock-on electrons. The most energetic electrons may escape the detector, depending on the energy of the incident particle as well as on the detector’s size and geometry. The energy deposited in a detector may therefore be less than the energy lost by the particle. This distinction can be an important distinction in some applications.

Figure 1 shows energy deposited in 300  $\mu\text{m}$  of silicon as calculated with the Bethe-Bloch equation, plotted as a function of particle energy, for protons, helium ions, and carbon ions. Notice that if we look at a particular value of  $\Delta E$  on the y axis, that is, at a quantity that is measured, different ions can give the same value. For example, a relatively low-energy proton (at, say, 70 MeV) and a high-energy helium ion in the plateau region above 1000 MeV/nuc each deposit about 500 keV in a 300  $\mu\text{m}$  thick silicon detector, and cannot be distinguished on the basis of this one measurement.

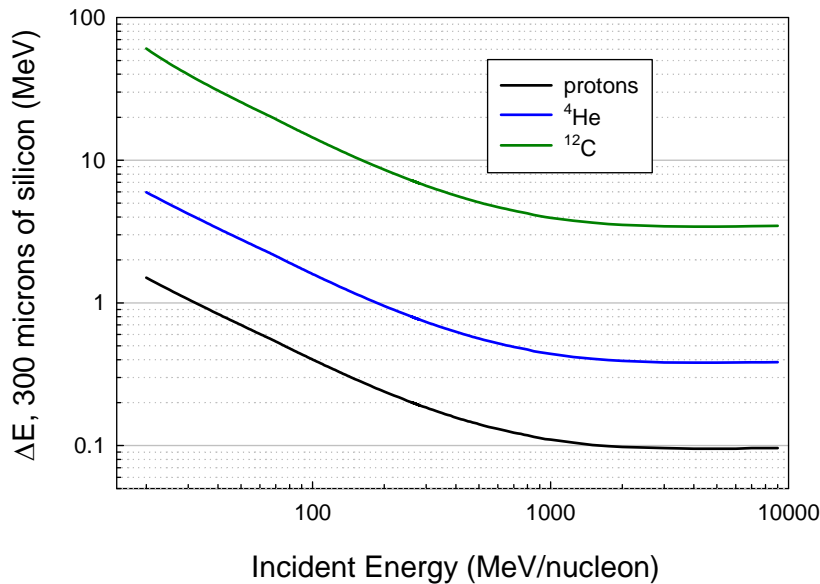


Figure 1. Energy lost in 300  $\mu\text{m}$  of silicon by protons, helium ions, and carbon ions, as functions of energy.

There is even some overlap of  $\Delta E$  between  $^4\text{He}$  at low energy and  $^{12}\text{C}$  ions in the plateau. Clearly, a more sophisticated approach to particle identification is needed.

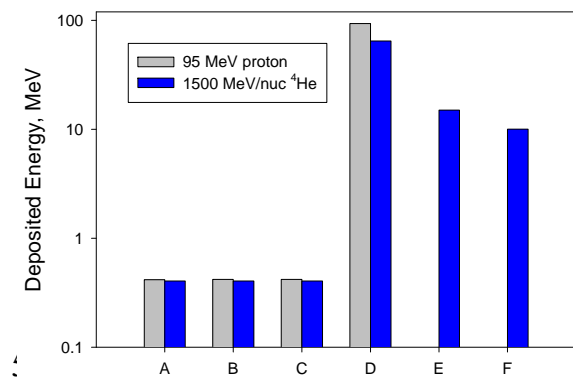


Figure 2. Calculated energy lost in the RAD detector stack by a 95 MeV proton and by a high-energy helium ion.

equation, plotted as a function of particle energy, for protons, helium ions, and carbon ions. Notice that if we look at a particular value of  $\Delta E$  on the y axis, that is, at a quantity that is measured, different ions can give the same value. For example, a relatively low-energy proton (at, say, 70 MeV) and a high-energy helium ion in the plateau region above 1000 MeV/nuc each deposit about 500 keV in a 300  $\mu\text{m}$  thick silicon detector, and cannot be distinguished on the basis of this one measurement.

Figure 2 shows a theoretical example based on the detector stack in the RAD instrument [11], which consists of three 300  $\mu\text{m}$  thick silicon detectors (known as the A, B, and C detectors), followed by a 2.8 cm thick cesium iodide scintillator (the D detector), a 1.8 cm thick plastic scintillator (E), and another 1.2 cm plastic scintillator (F). (See Figure 5 below for

details.) Shown are the calculated energy deposits from a proton that stops in the D detector, and from a helium ion that fully penetrates the detector stack. The deposited energies are nearly identical in detectors A through C, with a small difference in D. However, the proton stops in D and deposits no energy in E or F, whereas the helium ion continues through the stack and deposits substantial energy in both E and F. Thus, with multiple detectors and with sufficient detector mass, a particle of charge  $Z$  at fairly low energy can be unambiguously distinguished from a more energetic particle of charge  $Z + 1$ .

In a typical detector stack of modest depth, particles with energies high enough to be in the  $dE/dx$  plateau (i.e., where the curve is relatively flat) do not lose much of their energy. That is,  $dE/dx$  is nearly constant throughout the stack, and in these cases, even multiple measurements of deposited energy are not sufficient to determine the energy of the particle. Thus at high energy, only the charge can be inferred from  $\Delta E$ , and entirely different techniques are required to measure the energy. This fundamental behavior of charged particles in matter, combined with the stringent limits on mass that are usually imposed on flight detectors, makes precision measurements at high energies challenging. Furthermore, those same mass limits restrict the volume of practical flight detectors, which reduces the geometric factor (analogous to the “collecting power” of an optical telescope) that can be achieved. This in turn limits the statistical precision of measurements of heavy ions in the GCR. Solutions to these problems, including the use of very massive detectors, have been implemented, but the associated costs are high. A few examples of successful (and expensive) large flight detectors are given below. These include HEAO-C3 [12], PAMELA [13], AMS [14], and to a lesser extent, ACE/CRIS [15].

### Curvature in Magnetic Fields

A charged particle traversing a magnetic field is subject to a force, which in vector form is given by  $\mathbf{F} = d\mathbf{p}/dt = q \mathbf{v} \times \mathbf{B}$  where  $\mathbf{B}$  is the magnetic field vector,  $q$  is the charge of the particle, and  $\mathbf{p}$  is its momentum vector. In the plane transverse to the magnetic field vector, a charged particle follows a curving trajectory with radius  $\rho$  given by  $\rho = p/Bq$ . This convenient fact is commonly put to use in high-energy physics experiments with colliding beams, which typically have cylindrically-symmetric detector geometry and (in the modern era) a superconducting magnet in a solenoidal geometry that generates field lines parallel to the beam axis. Trajectories of particles emerging from collisions are bent in the plane perpendicular to the beam axis. Tracking chambers are used to measure curvature and hence momentum; this can be combined with  $dE/dx$  information for particle identification. In addition to their use in large ground-based experiments, a superconducting solenoidal magnet was flown on the balloon-borne cosmic ray detector BESS [16]. The AMS and PAMELA experiments use permanent magnets for tracking. The original design of AMS called for a superconducting magnet, but this was later abandoned due to thermal issues.

### Čerenkov radiation

Čerenkov radiation, sometimes called Čerenkov light, is electromagnetic radiation emitted when a charged particle passes through a dielectric medium (i.e., an insulator) at a speed greater than the speed of light in the medium. An energetic charged particle polarizes the molecules in the medium; they return nearly instantaneously (within 10 picoseconds) to their ground state by radiating photons at a characteristic angle  $\theta$  given simply by  $\cos(\theta) = 1/n\beta$ , where  $n$  is the index of refraction of the medium. In experimental particle physics, Čerenkov detectors of two basic types are used, those in which the cone of emitted light is measured (Ring Imaging Čerenkov, or RICH, detectors [17]), and threshold detectors, which simply determine whether a particle has a velocity greater or less than  $v = c/n$ . (Light is emitted only if  $v > c/n$ .) The number of photons generated in traversing a given length of material is proportional to  $(1-1/n^2\beta^2)$ , so that the amplitude of a pulse of Čerenkov light detected by (as in typical systems) a photomultiplier is related to the velocity.

Čerenkov detectors are commonly used when the energies of highly relativistic particles must be determined. They are also used in nuclear reactors, in ground-based systems that detect air showers initiated by very high-energy cosmic rays, and in large flight detectors, most notably the HEAO-3-C2 experiment, which will be discussed below. They are also used in ground-based arrays that detect air showers that are produced when ultra-high-energy cosmic rays enter Earth's atmosphere.

### Transition radiation

When a high-energy charged particle moves between one medium and another, it emits so-called "transition radiation" in the form of optical photons or x-rays [18]. The emitted light is a function of particle energy and its angle of emission is forward-peaked. The light yield is low and high photon detection efficiency is required. Transition radiation can be used to discriminate electrons from hadrons at very high energies. Like Čerenkov detectors, TRD's (transition radiation detectors) include both a radiator in which the photons are generated and a photodetector. Both the AMS and PAMELA instruments include TRD's.

## **Observables**

Before discussing measurement methods and devices, it is important to consider the physical quantities that one hopes to measure. Of greatest importance is the flux,  $J$ , of particles, which is defined as the number of particles crossing a unit area per unit solid angle per unit time. The most commonly used unit is particles per (cm<sup>2</sup> steradian sec), sometimes referred to as a particle flux unit or pfu. Differential flux – knowledge of which is needed for risk assessment calculations – is measured in energy bins and can be written  $dJ/dE$  with units of particles per

( $\text{cm}^2 \text{ sr s MeV}$ ). The counting rate of a detector is the product of  $J$  and the detector's geometry factor,  $G$ , which is given in units of  $\text{cm}^2 \text{ sr}$ , so that the counting rate,  $N$ , simply has units of  $\text{s}^{-1}$ . The geometry factor of any instrument is, to first order, simply a function of the telescope geometry. However  $G$  is typically understood to incorporate the detection efficiency, so that in general it is a complicated function of the charge, mass, and energy of the incident particles.

To calculate dose, flux is integrated over the time period of interest and over angles of incidence to get the fluence,  $\phi$ , which is typically given in units of particles per  $\text{cm}^2$ . In free space, the spatial integration goes over  $4\pi$  steradians; on a planetary surface, it goes over  $2\pi$ ; and in orbit around a large body, the solid angle subtended by the body (which may be a function of time) must be subtracted from  $4\pi$ . It is commonly assumed that the radiation field of interest is isotropic, so the integrations over solid angle are trivial. This is valid for the Galactic Cosmic Rays, and it is a good approximation for Solar Particle Events for some time after onset. However, in the initial stages of a SPE, particle distributions can be anisotropic; this complication is generally ignored in the absence of detailed information about the angular distribution of the incoming particles. Also, in Low-Earth Orbit (LEO), the radiation received in crossing of the South Atlantic Anomaly (SAA) is anisotropic.

At a fixed point in a mixed radiation field, the absorbed dose,  $D$ , is proportional to the sum (sometimes written as an integral) over all particles of LET multiplied by the fluence as a function of LET, i.e.,  $L \times \phi(L)$ . Absorbed dose is a purely physical quantity. The dose equivalent,  $H$ , a quantity to assess the risk of radiation exposure, is not purely physical – it takes into account the different degrees of biological effectiveness of different types of radiation. It is similarly calculated by summing over all particles the product  $L \times \phi(L) \times Q(L)$ , with the last quantity being the quality factor  $Q$ , which is defined [19] to be solely a function of  $L$ . In a mixed radiation field, accurately measuring the dose and dose equivalent requires that the LET distribution at the point of interest is well measured. Statistical and systematic uncertainties in the measurement of the LET spectrum propagate into uncertainties in  $D$  and  $H$ . Furthermore, typical flight dosimeters measure one spatial point at a time, but in general the LET distribution inside a spacecraft or inside an astronaut is position-dependent, due to anisotropies in the shielding distribution, source distribution, or both. The power of transport models lies in their ability to predict LET distributions at arbitrary points. There are several variations on dose equivalent; a useful list of definitions is given by Newhauser and Durante [20].

Transport model accuracy requires accurate underlying models of the relevant interactions (electromagnetic and nuclear) that occur as energetic particles penetrate matter. Such calculations begin with an initial distribution of incident particles and energies. The initial

distributions are based on empirical data that, at a minimum, must specify the differential fluxes as functions of charge and energy. Shielding then modifies the incident particle fluxes in complex ways. The entire enterprise of evaluating radiation dose, dose equivalent, and ultimately, risk to humans, rests on a foundation of accurate measurements of the fluxes of charged particles in space. In unshielded deep space, the flux is due to GCRs and sporadic SPE's. In low-Earth orbit, there are additional large contributions from trapped protons and electrons, particularly those in the South Atlantic Anomaly, and there is also a filtering effect due to the magnetic field. All these components must be accurately modeled in transport codes, or we can have no expectation of accurate dose predictions from the codes.

Note that the LET distribution, and hence the dose and dose equivalent, can be calculated starting with measurements of flux. In contrast, one cannot go the other way; that is, it is not in general possible to go from a measurement of dose (or LET) to flux.

## **Charged Particle Detection**

The exact type or types of detectors employed in a particular experiment depend entirely on the goals, size, and complexity of the experiment. Virtually all the measurement techniques employed in large-scale ground-based particle detectors have also been employed in flight instruments. For the sake of brevity, only the most common are described here.

### *Organic Scintillators*

Certain liquids and plastics such as polystyrene emit flashes of light when traversed by charged particles. Decades of research have yielded a large number of variants, as one can see by glancing through manufacturer's catalogs [21, 22]. In general, signals from plastic scintillators are very fast (rise times on the order of nanoseconds), but unfortunately their light outputs ( $dL/dx$ ) tend to be non-linear with deposited energy ( $dE/dx$ ) for protons and other ions. Light output is much more linear for electrons and  $\gamma$ -rays.

Scintillation light from either organic or inorganic scintillators is most commonly collected with photomultiplier tubes (gains of  $10^4$ - $10^6$ ), although other photosensors are used, including silicon photodiodes (which have no gain and are not suitable for low-light applications), avalanche photodiodes (gains of  $10^3$ - $10^4$ ), and highly pixellated avalanche photodiodes sometimes called silicon photomultipliers.

Because of their fast rise time, signals from plastic scintillators are commonly used for time-of-flight (ToF) measurements in ground-based detectors. Measuring flight time between points separated by a known distance gives a direct measurement of velocity. However, to be useful for

relativistic particles, this technique requires flight paths that are too long for the typical compact instruments used in spaceflight. Larger instruments, however, can accommodate such systems. For example, the ToF subsystem of the PAMELA detector uses plastic scintillators separated by 77.3 cm. AMS also has a ToF system with a flight path of 120 cm.

The non-linearity of scintillator light output with deposited energy is known as quenching. Briefly, the light yield of the scintillator is affected by details of the track structure, with the underlying cause being the re-absorption of energy in regions of dense ionization (e.g., along the central region of a heavy ion). A phenomenological description relating  $dL/dx$  to  $dE/dx$  was first provided by Birks [23], and other variants of his formula [24] have been developed to explain this complex behavior, which in principle depends on the charge and energy of the particle.

Plastic scintillators also are useful as neutron detectors. Polystyrene and polyvinyltoluene, the main constituents of plastic scintillators, both consist of approximately equal parts carbon and hydrogen. A neutron traversing a plastic scintillator can interact with either a carbon nucleus or hydrogen nucleus (i.e., a proton), but it is in the latter type of interaction that the neutron can efficiently transfer significant kinetic energy. The resulting recoil proton creates scintillation light. If enough interactions take place, virtually all of the neutron energy can be transferred to recoil protons; and if an isotope such as  ${}^6\text{Li}$ ,  ${}^{10}\text{B}$ , or  ${}^{157}\text{Gd}$  is present in the scintillator [25], a nuclear capture reaction is possible. In these instances, the amplitude of the light pulse from the recoil protons is approximately proportional to the energy of the incident neutron, and a second light pulse of characteristic amplitude is produced by the capture reaction. The coincidence of two pulses within a few microseconds (the average time required for the neutron to be captured) indicates that virtually all the neutron energy has been absorbed in the scintillator. This double-pulse method has been used in flight instruments flown to Mars [26] and Mercury [27]; a similar instrument will be flown to measure neutron dose on the International Space Station [28].

Plastic scintillators have also found use both in space and in high-energy physics in the form of so-called scintillating fiber detectors. A notable example of this type of detector is the one in the ACE/CRIS instrument. The scintillating fiber tracker is used for trajectory reconstruction, which is used in combination with data from silicon detector to obtain high-resolution energy measurements for GCR ions in the energy range most affected by solar modulation.

### *Inorganic Scintillators*

Many inorganic crystalline materials emit scintillation light when traversed by charged particles. While typical organic scintillators have densities on the order of  $1 \text{ g cm}^{-3}$ , common inorganic scintillators have considerably higher densities [29], ranging from about  $3.7 \text{ g cm}^{-3}$  for NaI to  $7.1 \text{ g cm}^{-3}$  for BGO. This increases the energy for which a scintillator of a given size can bring

an incident charged particle to rest. By stopping a charged particle, one obtains a measurement of its total energy,  $E_{\text{tot}}$ , which enables particle identification by the  $\Delta E$ - $E_{\text{tot}}$  method [30]. Like organic scintillators, inorganic scintillators also suffer from quenching, but to a lesser degree. Inorganic scintillators have the additional feature of relatively large efficiencies for detecting the full energy of gamma rays, making them useful for spectroscopic measurements in space.

### *Plastic Track Detectors and Thermoluminescence Detectors (TLDs)*

Plastic nuclear track detectors (PNTDs) have been used in spaceflight for several decades. An overview of the material properties and capabilities of CR-39, a specific and widely-used type of PNTD, can be found in an article by Cartwright et al. [7] Track detectors are passive devices that incur radiation damage when traversed by charged particles. After chemical etching of the surface, a track detector reveals, under high magnification, “pits” produced by the charged particles. Practical considerations typically limit the sensitive range of these detectors to LET values above about 5 keV/ $\mu\text{m}$ , far higher than the LET of the most common GCR particles. (Protons and helium ions with energies of several hundred MeV/nuc and higher have LET’s less than 2 keV/ $\mu\text{m}$ ). While the high LET threshold is a significant disadvantage, PNTDs can be used in conjunction with thermoluminescent dosimeters (TLDs), which tend to be less sensitive at high LET, to produce a combined response that covers the full range of interest in flight [32]. The capability of PNTDs to measure very short-ranged particles with very high LETs is unique among flight detectors. These particles, generally “target fragments” produced in nuclear interactions of high-energy particles, have very short ranges. If produced in the external environment, they only contribute to skin dose. However they are also produced by nuclear interactions inside the body and may contribute significantly to organ doses.

PNTD’s are etched and scanned some time (weeks or months) after exposure. Similarly, TLD’s are usually read out via a process of heating, which induces luminescence. The integrated light output is related to the ionizing radiation dose. Obviously, these are not “real-time” detectors. Rather, they provide historical records, integrated over the full time of exposure. The Pille system used on ISS [33] is an exception to this; it provides in-flight readout of TLD’s, allowing updates to astronaut dose records on comparatively short timescales. Dose measurements from TLD’s and PNTD’s continue to be of primary importance for monitoring astronaut exposures on the ISS.

TLD’s are crystalline materials. The most common TLD’s are made of lithium fluoride doped with magnesium and titanium. Like PNTD’s, TLD’s have been used in space since the 1960’s [34]. When ionizing radiation traverses a TLD, electrons are liberated and some are trapped by atoms of the first dopant. When the material is heated, some time after exposure, these electrons are liberated and then re-captured by the second dopant, releasing photons which are then

detected by a photosensor. The number of photons released is proportional to the absorbed dose recorded by the TLD.

TLD's and PNTD's have varying sensitivities to charged and neutral particles, depending on the details of their composition and (in the case of PNTD's) processing. A more detailed discussion of passive detectors is beyond the scope of this article. More information about TLD's can be found in the article by Benton and Benton [32].

### *Tissue-Equivalent Proportional Counters*

Tissue-Equivalent Proportional Counters, or TEPC's, are a standard instrument in health physics. There are several common designs, the first and still most-used being the Rossi chamber [35]. The Rossi chamber consists of a spherical cavity filled with tissue-equivalent gas at low pressure to simulate a diameter on the order of 1  $\mu\text{m}$ , on the same scale as the nucleus of a mammalian cell. The cavity is defined by a spherical wall of tissue-equivalent plastic. A wire, which typically is biased to a positive potential of several hundred volts, runs along a diameter of the sphere. Ionization electrons liberated by charged particles traverse the cavity, drifting towards the central wire, and when they are within several hundred nanometers of the wire, produce an avalanche of electrons that are collected on the wire. In the Rossi design, a uniform response independent of the direction of the incident particle is obtained by creating a cylindrically-symmetric electric field inside the avalanche region. This field is generated by a helical wire placed around the anode wire. Alternatively, a cylindrical chamber can be built, and no helical wire is needed, which creates a mechanically robust instrument compared to the fragility of the Rossi chamber. However, the chord length distribution of a cylindrical detector is somewhat more complicated than for the case of a spherical detector. TEPC's used to date on the Shuttle and ISS have been of the cylindrical variety, though a newer design being built by NASA JSC uses a spherical geometry without the need for helical wires by applying varying potentials to the segmented tissue-equivalent plastic wall.

TEPC's have several useful properties, the most notable of which is that they are relatively simple devices with one or two readout channels, yet they are capable of measuring both dose and LET spectra in real time with reasonable accuracy. (To be formally correct, TEPC's measure lineal energy, not LET.) TEPC's play a key role in dosimetry for NASA's human spaceflight program. The electronics used to read out TEPC signals are similar to those used for silicon detectors, described below.

### *Silicon Detectors*

A simple and robust particle detector can be made from a silicon diode with reverse bias voltage applied [36]. Silicon detectors generally have a planar structure. They are compact, can

withstand considerable doses of radiation, perform stably over a wide range of temperatures, require modest bias voltages for depletion, and can be built in a variety of shapes and sizes. The many virtues of silicon detectors have led to their widespread use in flight experiments that measure cosmic rays. Perhaps the pre-eminent example of a robust, long-running flight experiment is the silicon detector telescope [37] onboard the Voyager 2 spacecraft. The silicon detectors, fabricated in the Solid State Detector Lab at Lawrence Berkeley Laboratory in the 1970's, continue to function after nearly three decades in space. Detectors from the same lab were also used in a ground-based program of nuclear fragmentation measurements pertinent to NASA's Space Radiation Health Program [38]. Silicon detectors have been widely used in flight instruments.

When proper depletion voltage is applied, a silicon diode behaves in a manner similar to a parallel-plate ionization chamber. That is, the two end plates are at opposite polarities, and when a charged particle passes through the silicon, electrons migrate to the anode and holes to the cathode. Typically, the electrons – which have a higher velocity through the medium – are detected and integrated on a capacitor that forms part of the feedback of the “charge-sensitive” preamplifier. The amplitude of the output pulse is therefore linear with the charge liberated in the detector. One electron/hole pair is created per 3.6 eV of energy deposited. The best commercial preamplifiers have noise levels on the order of 100 electrons RMS [39], so that in principle, energy depositions as small as a few keV can be detected. In practice, this is rarely feasible due to other noise sources, but for example in the RAD instrument, energy depositions of a few tens of keV are seen above noise in silicon detectors that are 300  $\mu\text{m}$  thick.

The charge pulse from a silicon detector is usually integrated on the feedback capacitor of a “charge-sensitive” preamplifier, which is in essence a charge-to-voltage converter. The preamp output is typically passed through a Gaussian shaping amplifier and the peak voltage is digitized. The resulting digital value is linearly proportional to the energy deposited in the silicon. This can in turn be related to the charge, and in some cases the charge and energy, of the incident particle as described above in the discussion of the Bethe-Bloch formula.

### *Čerenkov Radiation Detectors*

When one wishes to know the energies of particles in the plateau of the Bragg curve [40], that is, of high-energy particles, methods other than the measurement of ionization energy loss are needed. Čerenkov detectors and transition radiation detectors are suitable for this purpose. Čerenkov detectors contain both a radiator – through which the incident particles pass and in so doing produce Čerenkov light – and a photodetector to record the light. Because the number of Čerenkov photons produced is typically small, the preferred photodetector for this application is the photomultiplier tube (PMT). PMT's are used in this application because they have high gain

and are therefore sensitive to very low light levels. Transition radiation detectors are conceptually similar.

### Ground-Based Air Shower Detectors

In recent decades, a new branch of cosmic-ray physics has emerged: the study of ultra-high-energy cosmic rays (UHECR). These rare particles – generally protons – are detected by means of large, elaborate ground-based detectors [41, 42] that record the showers of charged particles and/or Čerenkov radiation produced when these particles enter Earth’s atmosphere. These measurements aim to determine the full energy of the incident proton, which can exceed  $10^{20}$  eV. These particles are extremely scarce: they arrive at the top of the atmosphere at a rate of about one per square kilometer per year.

## **Neutron Detection**

The contribution to dose equivalent from neutrons can be significant in shielded environments. In particular, so-called fast neutrons in the range from about 100 keV to 10 MeV have large biological weighting factors [19]. Neutrons in this range are copiously produced when high-energy charged particles traverse significant depths of matter. The most important mechanism for their production is nuclear interaction between the incoming projectile (for instance, a high-energy GCR ion) and a nucleus of the material being traversed (e.g., the hull of a spacecraft). The primary source of neutrons below 10 MeV are nuclear interactions that leave the target nucleus in an excited state, which decays to a more stable state by “evaporation” of neutrons, protons, and heavier charged particles. Typically, these particles have energies on the order of a few MeV. At such low energies, the charged particles have negligible range, and for the most part come to rest near the point at which they were created. In contrast, neutrons do not undergo ionization energy loss, and those emitted in the evaporation stage can easily escape the material in which they were produced. They therefore get through shielding, and deliver dose inside even well-shielded habitats. Once in tissue, they undergo additional interactions and transfer their energy to nuclei in the body, producing short-ranged, high-LET tracks in tissue. Neutrons, somewhat paradoxically, are thus a source of high LET radiation despite the fact that they do not lose energy through ionization.

The fundamental properties of neutrons make it more difficult to detect them than it is to detect charged particles. Many methods have been implemented, but efficiency is always an issue since there is no direct detection. As mentioned previously, plastic scintillators are often used as neutron detectors, and this is true of instruments used in planetary science investigations as well [25, 26]. Another type of neutron detector flown on planetary missions is the  $^3\text{He}$ -filled proportional counter [43, 44]. In the realm of human spaceflight, neutron dosimetry has been

somewhat limited due to the difficulties noted above in detecting neutrons, and due to the fact that the neutron dosimeters flown to date have been sensitive to a limited range in neutron energies. For routine monitoring, the sensitivity of TLD's to neutrons can be enhanced by the addition of  $^6\text{Li}$  [45], which has a reasonably large neutron capture cross section. Isotopically enriched lithium [46] or boron can also be added to scintillators to achieve improved response to thermal neutrons.

## Calibration

Several methods can be used to calibrate instruments that are to fly in space. Details depend, of course, on the exact nature of the instrument. Beams of GCR-like ions produced in accelerators are generally of highest importance. Available facilities for such beams include the NSRL at Brookhaven National Laboratory [47], HIMAC in Chiba, Japan [48], and GSI in Darmstadt, Germany [49]. Neutrons are also important for calibration. High-energy neutron beam facilities for calibration include PTB in Braunschweig, Germany [50] and PSI in Uppsala, Sweden [51].

Laboratory sources can also play a useful role in calibration, as can the cosmic-ray muons that reach the Earth's surface. The latter provide a source of highly energetic and hence minimum-ionizing particles. Their energy deposition is essentially the same as that of the high-energy GCR protons that are abundant in space. Therefore demonstrating the ability to detect sea-level muons serves as verification that a flight instrument will detect the most common GCR ions. Additional circuitry for pulser-based calibration of amplifiers and analog-to-digital converters is also commonly built in to flight instruments.

There is no laboratory source that can produce highly-penetrating, medium- or high-LET particle radiation. Such particles make large contributions to dose and dose equivalent in space. Therefore it is extremely useful to be able to calibrate a detector system with similar particles in a ground-based setting such as the NSRL. This is particularly important for an instrument that (like RAD, for example) employs scintillators, which have a non-linear response to heavy ions. That is, because of quenching effects, the light output of a scintillation detector is not linearly proportional to the energy deposited. (This is in contrast to silicon detectors, which have a highly linear response.) Using a variety of heavy ion beams and energies allows one to map out the non-linearities in the response.

## A Brief Tour of Cosmic Ray Detectors

Many types of particle detectors have been devised over the last century. Virtually all of them have, in one form or another, been applied to the study of cosmic rays. A detailed description is

not in order here, but interested readers may pursue the references. Detector types that have been used to study cosmic rays, but that are not specifically described in more detail below, include electrometers [52], Geiger-Mueller counters [53], ionization chambers [54], cloud chambers [55], nuclear emulsions [56], and bubble chambers [57]. For example, the discovery of the Van Allen belts [3] was made using a simple Geiger tube capable of detecting protons with energies above 30 MeV and electrons above 3 MeV. The following sections describe several instruments that have flown in more recent times. The instruments included in the discussion do not by any means represent an exhaustive list; however, they have all played (or currently play) a significant role in our understanding of the health risks of extraterrestrial environments.

### GOES

The GOES (Geostationary Operational Environmental Satellite) program has been flying particle detectors in geostationary orbit for decades. GOES spacecraft contain instrument suites intended to measure a variety of phenomena [58]. The instruments include x-ray and energetic particle detectors that have proven to be extremely useful for the study of SPEs. Real-time GOES data are used to monitor ambient conditions for the ISS [59]. A three-day plot of proton fluxes is available online in real time, updating every five minutes [60]. The three time series displayed in the online monitor are integral fluxes of protons with energies above 10, 50, and 100 MeV. More detailed data are given in archived text-format files that are also freely available. Differential proton fluxes are given in 10 channels from 0.7 MeV to 700 MeV. The integral flux for protons above 700 MeV is also given. Questions have been raised about the calibration and absolute normalization of GOES energetic particle data [61].

### ACE/CRIS

The Advanced Composition Explorer (ACE) spacecraft sits at the L1 point, where it measures a wide variety of charged particles, including comparatively low-energy solar wind ions and electrons. Of interest here is the Cosmic Ray Isotope Spectrometer (CRIS), which has been measuring GCRs from Be (charge 4) to Ni (charge 28) since 1997 [62, 63]. CRIS contains several identical stacks of thick silicon detectors which stop GCR ions with energies up to a few hundred MeV/nucleon. The exact stopping energy is a function of the charge and mass of the ion. For example, boron ions are stopped at energies up to 173.7 MeV/nuc, while Fe ions stop at energies up to 471 MeV/nuc. Scintillating fiber trackers upstream of each silicon detector stack determine the incident angle, improving the precision of the measurement. CRIS measures GCR ions in the energy range in which solar modulation is most important, and its operational life is well into its second solar cycle. The outstanding design and performance of the CRIS instrument are enabled by relatively generous mass and power allocations: 30.4 kg and 12 W (16 W peak), respectively. This is far more resource-intensive than compact instruments such as RAD (1.6 kg,

4 W) and CRaTER (5.5 kg, 6.7 W). For well-designed instruments, greater mass and power equate to superior capability and performance.

### HEAO-3-C2

Three spacecraft were flown bearing the name “High Energy Astrophysics Observatory,” abbreviated to HEAO [64]. The third, HEAO-3, was launched in 1979 and contained an instrument known as C2, or HEAO-3-C2 in full. This instrument, built by French and Danish scientists, was largely based on Čerenkov detectors [12] and a time-of-flight system. The data from this instrument yielded the best measurements of GCRs in the 0.6 to 35 GeV/nucleon range made to date. At these energies, solar modulation of the GCR is negligible, so that the fluxes reported by the HEAO-3-C2 team [65] are expected to be nearly constant. The HEAO-3-C2 data at high energy, combined with the ACE/CRIS data in the lower-energy regime that is sensitive to solar modulation, provide a complete, time-dependent picture of the GCR in the energy range that is most important for humans in space.

The HEAO-C3 experiment operated from October 1979 to June 1980. Good statistics were obtained in a short time because the geometry factor of the detector was large, about 700 cm<sup>2</sup> sr, about double that of the ACE/CRIS instrument. The mass and power consumption of the instrument were similarly large: 350 kg, and 35 W. For comparison, the RAD and CRaTER instruments have geometry factors on the order of 1 cm<sup>2</sup> sr.

### MARIE

In contrast to the massive HEAO-3-C2 instrument, and the less massive but still quite large ACE/CRIS instrument, the MArTian Radiation envIronment Experiment (MARIE) [66] was very compact, with a mass of 3.3 kg and a modest power consumption of 4 W. MARIE was selected for the 2001 Mars Odyssey mission, which began science operations in Mars orbit in early 2002. MARIE operated successfully for 20 months, providing the first detailed radiation data from Mars. MARIE failed in the huge solar storm of October 2003, presumably due to a fatal latch-up in the electronics. In addition to a somewhat standard silicon detector stack, MARIE’s design incorporated a couple of clever innovations: a pair of silicon strip detectors to measure angles of incidence for ions in the telescope’s field of view, and a Čerenkov detector located at the bottom of the stack to provide velocity measurements. Due to severe budget and time pressures, these systems were not optimized and did not yield useable flight data. However, the silicon detector stack worked to measure GCR fluxes in the charge range from 2 to 11, as well as several SPEs [67].

MARIE’s design concept was sound, but implementation – particularly in the instrument’s electronics – was less than ideal. The resulting issues have been described in the literature [67].

They include electronic saturation at a signal level that is small compared to the levels caused by heavy ions in the GCR, and a very limited rate at which the data acquisition system could run without corrupting the data (less than 3 Hz). These problems would have been obvious, and to a large extent correctable, if adequate testing had been done during the development of the instrument. The history of the MARIE instrument provides an object lesson in the absolute necessity for functional testing and calibration of flight instruments with particle beams, and in the need for extreme care in the choice of electronic parts, which must be able to withstand significant radiation doses.

### CRaTER

The Cosmic Ray Telescope for the Effects of Radiation (CRaTER) instrument is currently flying in lunar orbit aboard the LRO spacecraft [68, 69]. CRaTER is also a modestly-sized instrument, with a mass of 5.5 kg and a power consumption of 6.7 W. A sketch is shown in Figure 3. The design of the instrument features an innovative design based on a silicon detector telescope in a unique configuration. The instrument contains six detectors, mounted in three pairs. In each pair,

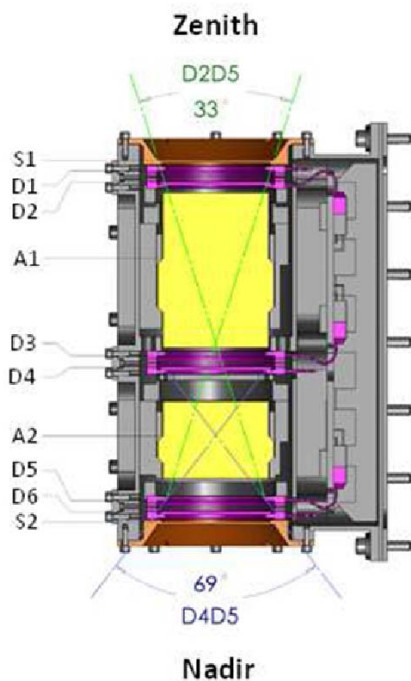
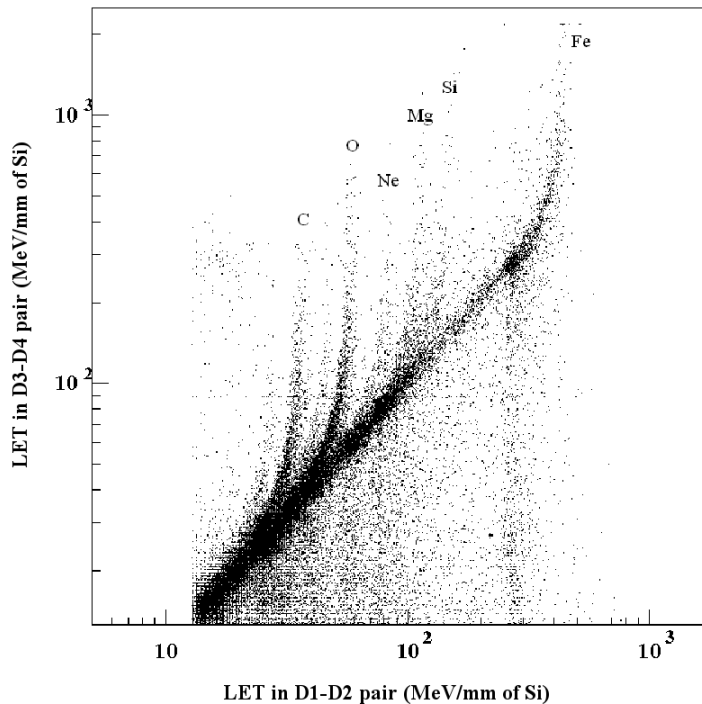


Figure 3. Schematic drawing of the CRaTER instrument.

there is a thin detector (150  $\mu\text{m}$ ) and a thick detector (1 mm). The first pair is mounted at one end of the telescope, which points towards the zenith. In between the first and second pairs is a thick piece of tissue-equivalent plastic (TEP), amounting to about  $6 \text{ g cm}^{-2}$  of areal density. This depth is comparable to that of the blood-forming organs in humans. Thus while the first detector pair is good for characterizing the incident radiation, the second detector pair measures at a depth that is of interest for understanding self-shielding of the body. The second and third detector pairs are separated by an additional piece of TEP, about  $3 \text{ g cm}^{-2}$  deep. The third pair provides additional information about the depth-dose relation, and also detects charged particles coming up from the Moon. (The third pair is nadir-pointing – the surface of the Moon entirely fills its field of view in the nominal mapping orbit 50 km up.) These “albedo” particles are produced when high-energy cosmic rays undergo nuclear interactions in the top layer of lunar soil.

In addition to acting as shielding, the two TEP blocks in CRaTER (TEP1 and TEP2) give the instrument some interesting performance characteristics relative to other small instruments.

Figure 4 shows a scatter plot of deposited energy per unit detector depth in the second detector pair (D3-D4) vs. that in the first detector pair (D1-D2). The upward-curving bands are due to ions that lose considerable energy in TEP1. The bands below the 45° line are due to fragmentation of the incident ions in the TEP.



*Figure 4. CRaTER data showing the influence of TEP on heavy ion energy deposition. Detectors D1 and D2 are ahead of the first piece of TEP, detectors D3 and D4 are just behind it. In this plot, cuts have been applied to the data to require energy deposition corresponding to carbon ions or heavier in both detector pairs.*

### *RAD for the Mars Science Laboratory (MSL) Mission*

The RAD instrument is, as of this writing, on its way to Mars aboard the MSL spacecraft. Landing is scheduled for August 6, 2012. RAD represents a significant technological advance over MARIE, the previous particle instrument sent to Mars. MARIE operated in orbit around Mars; RAD will make the first measurements of the surface radiation environment. Because there is expected to be a significant contribution from neutrons on the surface, RAD must be able to measure these particles and to discriminate against charged particles. It must also measure the full range of charged particles, which requires a dynamic range of about 10<sup>4</sup>:1. All this capability must be contained in a package with a mass as close to 1 kg as possible. These challenging requirements were met by modifying a particle telescope designed for the Solar Orbiter mission [70]. The major modifications for RAD as built for the MSL mission – shown schematically in Figure 5 – are that the “E” detector (used primarily for neutron detection) is now below the “D” detector instead of off to the side, and a single anticoincidence shield surrounds both D and E. This anticoincidence shield allows us to reject sideways-going charged particles that deposit

Reviewed

Posted to THREE April 30, 2012

energy in D and/or E but that are outside the field of view of the A-B-C detector stack. A, B, and C are 300  $\mu\text{m}$  thick silicon detectors with extremely low noise and wide dynamic range in their readout electronics; D is a CsI(Tl) scintillating crystal, and both E and the anticoincidence shield are Bicron BC-432 plastic scintillator. The “A” detector is split into outer (A1) and inner (A2) rings. All scintillators in RAD are read out by photodiodes. Using photodiodes means there is only a single high-voltage power supply, which runs at 70 V. This relatively low voltage mitigates the possibility of coronal discharge from a power supply running at higher voltage (which would be needed, for example, if a photomultiplier tube or a TEPC-type detector were employed). Coronal discharge is a serious issue at the low atmospheric pressure on the Martian surface. Using photodiodes also keeps the design compact and minimizes mass.

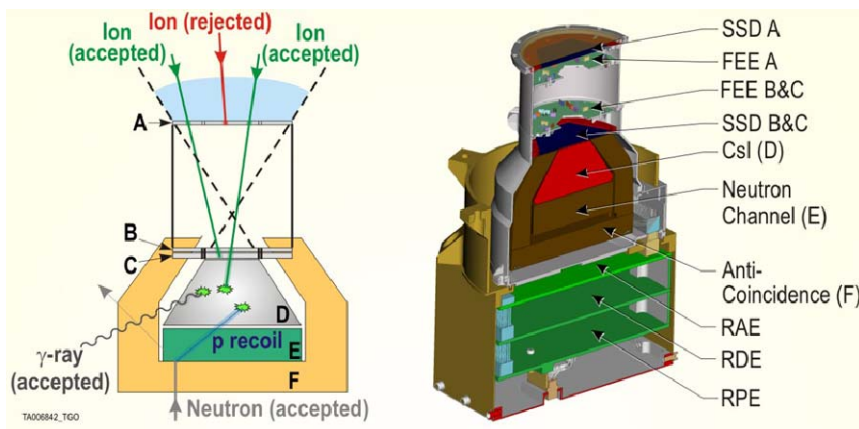


Figure 5. Schematic drawing of RAD (right) and its methods of charged and neutral particle detection and discrimination (left).

Owing both to the mass limitations and the fact that the MSL rover is powered by a radioisotope thermal generator (RTG) that produces a large background of neutral particles, detection of neutrals in RAD is challenging. (Neutral particle events are defined as those with significant deposited energy in D and/or E but not in F.) At low energies, below about 5 MeV, neutrons and  $\gamma$ -rays from the RTG are expected to dominate over the neutrons coming from the surface environment. Thresholds are set accordingly. For higher energies, RAD's efficiency falls off when proton recoils are sufficiently energetic to escape from E and hit the anti-coincidence. (Such events cannot be distinguished from charged particles coming from the side or from the surface of Mars.) In between, in the neutron energy range from about 5 to  $\sim 100$  MeV, RAD is reasonably efficient. The combined neutron and gamma spectra can be unfolded, as shown by Kohler et al [71] for energies up to 19 MeV. Work is underway to test this method at neutron energies up to 70 MeV.

The RAD sensor head contains the detectors and front-end electronics (preamplifiers and first-stage shaping amplifiers). Signals from the sensor head go to the electronics box. The electronics box contains three circuit boards, one of which is the analog electronics board that processes the signals delivered by the sensor head. At the heart of the analog electronics board is the VIRENA [72], a custom 36-channel ASIC that processes the analog signals. The sensor head sends 17

Reviewed

Posted to THREE April 30, 2012

analog signals to the VIRENA – two each from A1, A2, B, and C; three each from D and E; and three anti-coincidence signals. Each of the 17 is input into two VIRENA channels for the sake of redundancy, with two VIRENA channels to spare. Each VIRENA channel contains additional amplifiers, discriminators, and sample-and-hold circuitry. The VIRENA outputs are digitized by a 14-bit analog-to-digital converter. RAD contains three processors, one of which handles communications with the rover's computer, one to control the VIRENA, and the third to perform the data processing tasks.

RAD has been extensively tested and calibrated in a wide range of particle beams, including protons at energies from 100 to 1000 MeV, helium, carbon, neon, silicon, and iron beams at energies from a few hundred MeV/nuc up to 1000 MeV/nuc, the range of greatest importance for dosimetry in space. RAD has also been tested in monoenergetic neutron beams at 5, 15, and 19 MeV and in an AmBe source field. Further testing at higher neutron energies, in the 20 to 80 MeV range [51] was performed post-launch using the flight spare unit. The large volume of data acquired in the calibration campaign allows for accurate calibration, including calibration of the scintillators which have a non-linear response due to quenching. Accurate calibration is needed because much of RAD's data processing is done in real time in the instrument, and the processing requires knowledge of actual energy deposited in the individual detectors (not just pulse heights as measured by the ADC). This is necessary because RAD's telemetry allocation is quite small and the data must be made as compact as possible. This is achieved by assigning most events to histograms and only storing a subset of pulse-height (list mode) event records.

### *RAD for the ISS*

In shielded environments such as the International Space Station (ISS), neutrons with about 1 MeV of kinetic energy can make a significant contribution to dose and dose equivalent. These neutrons are secondary particles produced in the interaction of higher-energy charged particles. Because neutrons do not lose energy through ionization, they can penetrate large depths of shielding, including human tissue. When they interact, neutrons tend to produce short-ranged interaction products with high LET and hence large quality factors. These interactions can be either elastic (e.g., the creation of a recoil proton when a neutron collides with a hydrogen nucleus) or inelastic (e.g., fragmentation of a heavier nucleus such as carbon). Therefore it is important – though difficult – to measure neutrons in the energy range from about 500 keV to 10 MeV. A version of the MSL-RAD instrument is currently being built for the ISS. It will contain a near-copy of the MSL-RAD system described above (sensor head plus electronics box) as well as a separate “Fast Neutron Detector” (FND) based on a boron-loaded plastic scintillator. The two parts will share a common data storage area and interface to the ISS. The FND will detect neutrons and measure their energy using the double-pulse method described above. The first

pulse is due to recoil protons, and is related to the energy of the incident neutron; the second pulse comes from the capture of the thermalized neutron by a  $^{10}\text{B}$  nucleus.

### Other Instruments

As stated at the outset of this section, the list of instruments given here is not intended to be complete, nor is any slight intended towards other instruments that have made historically-important measurements in space. There are simply too many such instruments to discuss here. A partial list of other important instruments includes the Voyager particle experiments [34], IMP-8 [73], SAMPEX [74, 75], the CO-SPIN experiment on Ulysses [76], and those aboard the two STEREO spacecraft [77]. Also, some key observations have come from ground-based neutron monitors [78, 79, 80], which indirectly measure cosmic-ray fluxes by means of the secondary neutrons they produce in the Earth's atmosphere.

### **Conclusions and Acknowledgments**

Of course, one cannot really do justice to such a vast subject area in an overview article such as this. I have accordingly tried to give references – with an emphasis on those that are freely available – sufficient to enable the interested reader to pursue any of the topics in much greater detail.

Careful and accurate measurements of the cosmic rays most important to human health in extraterrestrial environments have been, and continue to be, made. It is important to note that making these measurements requires a significant commitment of resources, not only in the form of funding but in the form of sufficient mass, power, and telemetry allocations for flight instruments. While we continue to learn much about solar modulation from the ongoing success of the ACE mission, and while we hope to learn about the radiation environment on the Martian surface from RAD, it is worth noting that GCR data of the highest importance were obtained in an eight-month interval more than thirty years ago (HEAO-3-C2). Arguably those measurements were made with such accuracy and precision, and are sufficiently immune to the effects of solar modulation, that they need not be repeated, but there are few ongoing scientific endeavors in which data of such a vintage are considered to be an undisputed gold standard.

## References

- [1] Hess's thoughts on cosmic rays 24 years after he discovered them, and a good picture of the state of knowledge in 1936, are captured in his Nobel Prize acceptance speech, reprinted here: [http://nobelprize.org/nobel\\_prizes/physics/laureates/1936/hess-lecture.html](http://nobelprize.org/nobel_prizes/physics/laureates/1936/hess-lecture.html)
- [2] H. L. Bradt and B. Peters, Investigation of the Primary Cosmic Radiation with Nuclear Photographic Emulsions, *Phys. Rev.* 74, 1828-1837 (1948).  
<http://link.aps.org/doi/10.1103/PhysRev.74.1828>
- [3] J. A. Van Allen, C. E. McIlwain, and G. H. Ludwig, Radiation Observations with Satellite 1958  $\epsilon$ , *J. Geophys. Res.* 64, No. 3, 271-286 (1959).  
<http://dx.doi.org/10.1029/JZ064i003p00271>
- [4] J. Linsley, Evidence for a Primary Cosmic-Ray Particle with Energy  $10^{20}$  eV, *Phys. Rev. Lett.* 10, 146 (1963). <http://dx.doi.org/10.1103/PhysRevLett.10.146>
- [5] M.F. Moyers, P. B. Saganti and G.A. Nelson; EVA space suit proton and electron threshold energy measurements by XCT and range shifting, *Rad Meas* 41 (9-10) 1216-1226, 2006.  
<http://dx.doi.org/10.1016/j.radmeas.2006.04.033>,
- [6] G. Reitz, EUROPEAN Dosimetry Activities for the ISS, *Physica Medica* XVII, Suppl. 1, 283-286 (2001). [http://www.physicamedica.com/VOLXVII\\_S1/77-REITZ.pdf](http://www.physicamedica.com/VOLXVII_S1/77-REITZ.pdf)
- [7] B. G. Cartwright, E. K. Shirk, and P. B. Price, A nuclear-track-recording polymer of unique sensitivity and resolution, *Nucl. Instr. Meth.* 153, 457-460 (1978).  
[http://dx.doi.org/10.1016/0029-554X\(78\)90989-8](http://dx.doi.org/10.1016/0029-554X(78)90989-8)
- [8] Y. S. Horowitz, *Thermoluminescence and Thermoluminescent Dosimetry*, v. 1, ICRC Press, Boca Raton, FL (1984).
- [9] Experiments conducted at the Large Hadron Collider are discussed here: <http://public.web.cern.ch/public/en/lhc/LHCExperiments-en.html> and at the links found there.
- [10] H. Bethe und J. Ashkin in *Experimental Nuclear Physics*, ed. E. Segré, J. Wiley, New York, p. 253 (1953).

[11] The Radiation Assessment Detector is part of the Mars Science Laboratory suite of instruments. <http://msl-scicorner.jpl.nasa.gov/Instruments/RAD/> Contact the author of this article for additional details.

[12] W.R. Binns et al., Abundances of ultraheavy elements in the cosmic radiation: Results from *HEAO 3*, *Astrophysical Journal*, 346, 997 (1989).  
<http://adsabs.harvard.edu/full/1989ApJ...346..997B>

[13] P. Picozza et al., PAMELA – A payload for antimatter exploration and light-nuclei astrophysics, *Astropart. Phys.* 27, 296-315 (2007).  
<http://dx.doi.org/10.1016/j.astropartphys.2006.12.002>

[14] The Alpha Magnetic Spectrometer is used on the International Space Station.  
[http://www.nasa.gov/mission\\_pages/station/research/experiments/AMS-02.html](http://www.nasa.gov/mission_pages/station/research/experiments/AMS-02.html)

[15] The Cosmic Ray Isotope Spectrometer is part of the instrument package on the Advanced Composition Explorer spacecraft. [http://www.srl.caltech.edu/ACE/CRIS\\_SIS/cris.html](http://www.srl.caltech.edu/ACE/CRIS_SIS/cris.html)

[16] Balloon-borne Experiment with Superconducting Spectrometer.  
<http://www.universe.nasa.gov/astroparticles/programs/bess/>

[17] Ring Imaging Cherenkov Detector (RICH detector).  
[http://en.wikipedia.org/wiki/Ring\\_imaging\\_Cherenkov\\_detector](http://en.wikipedia.org/wiki/Ring_imaging_Cherenkov_detector)

[18] Transition Radiation: The Relationship of Transition Radiation to X-ray Cherenkov Radiation  
<http://geant4.cern.ch/G4UsersDocuments/UsersGuides/PhysicsReferenceManual/html/node35.html>

[19] The 2007 Recommendations of the International Commission on Radiological Protection, ICRP Publication 103, Ann. ICRP 37 (2-4), 2007.

[20] W. D. Newhauser and M. Durante, Assessing the risk of second malignancies after modern radiotherapy, *Nat. Rev. Cancer* 11, 438-448 (2011). <http://dx.doi.org/10.1038/nrc3069>

[21] Scintillation products. <http://www.detectors.saint-gobain.com/uploadedFiles/SGdetectors/Documents/Brochures/Organics-Brochure.pdf>

[22] Scintillation products. <http://www.eljentechnology.com/>

24

Reviewed

Posted to THREE April 30, 2012

[23] J. B. Birks, *Theory and Practice of Scintillation Counting*, Pergamon Press, Oxford (1964).

[24] A. Menchaca-Rocha, A simplified scintillator-response formula for multiple-ion energy calibrations, *Nucl. Instr. Meth. Phys. Res. A* 602(2), 421-424 (2009).

<http://dx.doi.org/10.1016/j.nima.2009.01.190>

[25] V. B. Brudanin, Element-loaded organic scintillators for neutron and neutrino physics, *Phys. Part. Nuclei* 6 (109), 69 (2001). [http://dx.doi.org/10.1142/9789812811363\\_0080](http://dx.doi.org/10.1142/9789812811363_0080)

[26] R. S. Saunders et al., 2001 Mars Odyssey Mission Summary, *Space Science Reviews*. 110 (1-2), 37-83 (2004). <http://dx.doi.org/10.1023/B:SPAC.0000021006.84299.18>

[27] J. O. Goldsten et al., The MESSENGER Gamma-Ray and Neutron Spectrometer, *Space Science Reviews* 131 (1-4), 339-391 (2007). <http://dx.doi.org/10.1007/s11214-007-9262-7>

[28] A “Fast Neutron Detector” will be part of the ISS-RAD package currently in development. Contact the author of this article for further details.

[29] An excellent discussion of inorganic scintillators and their properties can be found here: <http://pdg.lbl.gov/2011/reviews/rpp2011-rev-particle-detectors-accel.pdf> (see Section 28 and Table 28.4 in particular).

[30] The ACE/CRIS and SIS instrument teams use this method, and give a clear explanation here: [http://www.srl.caltech.edu/ACE/CRIS\\_SIS/dedx.html](http://www.srl.caltech.edu/ACE/CRIS_SIS/dedx.html)

[32] E. R. Benton and E. V. Benton, Space radiation dosimetry in low-Earth orbit and beyond, *Nucl. Instr. And Meth. In Phys. Res. B* 184 (1-2), 255-294 (2001).

[http://dx.doi.org/10.1016/S0168-583X\(01\)00748-0](http://dx.doi.org/10.1016/S0168-583X(01)00748-0)

An example of the PNTD/TLD method on the ISS is given in

[http://wrmiss.org/workshops/thirteenth/Semones\\_STS120.pdf](http://wrmiss.org/workshops/thirteenth/Semones_STS120.pdf)

[33] P.P. Szabó, I. Fehér, S. Deme, B. Szabó, and J. Vágvölgyi, Dosimetric properties of the 'Pille' portable, wide dose range TLD reader, *Rad. Prot. Dosim.* 17 (1-4), 279-281 (1986).

<http://rpd.oxfordjournals.org/content/17/1-4/279.abstract>

[34] R.G. Richmond, Radiation dosimetry for the Gemini program, NASA Technical Note D-6695, 1972. [http://ntrs.nasa.gov/archive/nasa/casi.ntrs.nasa.gov/19720011147\\_1972011147.pdf](http://ntrs.nasa.gov/archive/nasa/casi.ntrs.nasa.gov/19720011147_1972011147.pdf)

25

Reviewed

Posted to THREE April 30, 2012

[35] H. H. Rossi and W. Rosenzweig, "A Device for the Measurement of Dose as a Function of Specific Ionization," *Radiology*, 64, 404 (1955). <http://dx.doi.org/10.1148/64.3.404>

[36] P.G. Eancoita and A. Seidman, Silicon detectors in high energy physics: physics and applications, *La Rivista del Nuovo Cimento* vol. 5, N. 7, 1-75 (1982). There are many introductory articles on silicon detectors, but this one is exceptionally thorough.  
<http://dx.doi.org/10.1007/BF02740017>

[37] E. C. Stone, R. E. Vogt, F. B. McDonald, B. J. Teegarden, J. H. Trainor, J. R. Jokipii, and W. R. Webber, "Cosmic Ray Investigation for the Voyager Missions: Energetic Particle Studies in the Outer Heliosphere - And Beyond," *Space Sci. Rev.*, Vol. 21, (3), p. 355, 1977.  
<http://dx.doi.org/10.1007/BF00211546>

[38] C. J. Zeitlin, K. A. Frankel, W. Gong, L. Heilbronn, E. J. Lampo, R. Leres, J. Miller, W. Schimmerling, A modular solid state detector for measuring high energy heavy ion fragmentation near the beam axis. *Radiation Measurements*, 23:65-81, 1994.  
[http://dx.doi.org/10.1016/1350-4487\(94\)90025-6](http://dx.doi.org/10.1016/1350-4487(94)90025-6)

The detectors described in this article were subsequently used to make a series of nuclear cross section measurements. Interested readers may contact the author for more information, reprints, etc.

[39] An example of a commercial preamplifier. <http://www.amptek.com/coolfet.html>

[40] Some examples of Bragg curves obtained at the NASA Space Radiation Laboratory (NSRL) may be found here: [http://www.bnl.gov/medical/NASA/CAD/Bragg\\_Curves.asp](http://www.bnl.gov/medical/NASA/CAD/Bragg_Curves.asp)

[41] H. Kawai et al., Telescope Array Experiment, Proceedings of the XIV International Symposium on Very High Energy Cosmic Ray Interactions *Nuc. Phys. B* 175-176, 221-226 (2008). <http://dx.doi.org/10.1016/j.nuclphysbps.2007.11.002>

[42] M. T. Dova et al., Survey of the Pierre Auger Observatory, in Proceedings of ICRC 2001, 699, available online: [http://www.auger.org/technical\\_info/pdfs/icrc2001/papers/ici7345\\_p.pdf](http://www.auger.org/technical_info/pdfs/icrc2001/papers/ici7345_p.pdf)

[43] The  $^3\text{He}$ -based detector flown on the Lunar Prospector mission is described here: <http://lunar.arc.nasa.gov/results/neutron.htm>

[44] R. S. Saunders et al., 2001 Mars Odyssey Mission Summary, *Space Science Reviews*. 110 (1-2), 37-83 (2004). <http://dx.doi.org/10.1023/B:SPAC.0000021006.84299.18>

The Russian HEND instrument aboard the 2001 Mars Odyssey spacecraft includes three  $^3\text{He}$  counters with varying amounts of polyethylene shielding which acts to moderate neutron energies.

[45] C. Furetta, *Handbook of Thermoluminescence*, World Scientific Publishing Co., 2010.

[46] A. R. Spowart, Measurement of the Absolute Scintillation Efficiency of Granular and Glass Neutron Scintillators, *Nucl. Instr. Meth.* 75, 35-42 (1969). [http://dx.doi.org/10.1016/0029-554X\(69\)90644-2](http://dx.doi.org/10.1016/0029-554X(69)90644-2)

[47] GCR-like ions are produced for the NASA Space Radiation Laboratory at the Brookhaven National Laboratory. [http://www.bnl.gov/medical/nasa/nsrl\\_description.asp](http://www.bnl.gov/medical/nasa/nsrl_description.asp)

[48] HIMAC is a heavy-ion synchrotron that was developed for medical use.  
<http://www.nirs.go.jp/ENG/facilt07.htm>

[49] GSI operates a unique large-scale accelerator for heavy ions.  
[http://www.gsi.de/portrait/ueberblick\\_e.html](http://www.gsi.de/portrait/ueberblick_e.html)

[50] Quasi-monoenergetic neutrons in the energy range between about 30 and 75 MeV can be produced for PTB in Braunschweig, Germany. <http://www.ptb.de/en/org/6/65/ucl.htm>

[51] The cyclotron at the the Svedberg Laboratory, Uppsala, Sweden includes a facility designed to produce high intensity, well-collimated and energetically well defined neutron beams in the energy region 20 – 180 MeV.  
<http://accelconf.web.cern.ch/AccelConf/e98/PAPERS/WEP04E.PDF>

[52] Electrometers measure electric charge or electric potential difference.  
<http://en.wikipedia.org/wiki/Electrometer>

[53] A Geiger counter is a type of particle detector used to detect or measure ionizing radiation.  
[http://en.wikipedia.org/wiki/Geiger\\_counter](http://en.wikipedia.org/wiki/Geiger_counter)

[54] An ionization chamber is a simple gas-filled detector that measures ionizing radiation.  
[http://en.wikipedia.org/wiki/Ionization\\_chamber](http://en.wikipedia.org/wiki/Ionization_chamber)

[55] A cloud chamber is a particle detector used to detect ionizing radiation.

[http://en.wikipedia.org/wiki/Cloud\\_chamber](http://en.wikipedia.org/wiki/Cloud_chamber)

[56] Nuclear emulsions are used to detect ionizing radiation.

<http://www.ilfordphoto.com/Webfiles/2006214150271441.pdf>

[57] A bubble chamber is a vessel filled with superheated liquid used to detect electrically charged particles moving through it. [http://en.wikipedia.org/wiki/Bubble\\_chamber](http://en.wikipedia.org/wiki/Bubble_chamber)

[58] The Geostationary Operational Environment Satellite program uses geosynchronous satellites to provide weather monitoring and forecasting data.

[http://en.wikipedia.org/wiki/Geostationary\\_Operational\\_Environmental\\_Satellite](http://en.wikipedia.org/wiki/Geostationary_Operational_Environmental_Satellite)

[59] NASA's Space Radiation and Analysis Group monitors space weather and its effects on space missions. <http://srag.jsc.nasa.gov/MissionSpaceWeather/SpaceWeather.cfm>

[60] Real-time space weather data is available online from the NOAA/Space Weather Prediction Center. [http://www.swpc.noaa.gov/rt\\_plots/pro\\_3d.html](http://www.swpc.noaa.gov/rt_plots/pro_3d.html)

[61] D. F. Smart and M. A. Shea, Comment on the use of GOES solar proton data and spectra in solar proton dose calculations, *Radiat. Meas.* 30, 327-335 (1999).

[http://dx.doi.org/10.1016/S1350-4487\(99\)00059-1](http://dx.doi.org/10.1016/S1350-4487(99)00059-1)

[62] E. C. Stone et al., The Cosmic Ray Isotope Spectrometer for the Advanced Composition Explorer, *Space Sci. Rev.* 86 (1-4), 285-355 (1998). <http://dx.doi.org/10.1023/A:1005075813033>

[63] The online data archive linked here allows one to view ion fluxes vs. time for selected species, going back to 1997. [http://www.srl.caltech.edu/ACE/ASC/level2/lvl2DATA\\_CRIS.html](http://www.srl.caltech.edu/ACE/ASC/level2/lvl2DATA_CRIS.html)

[64] The High Energy Astrophysics Observatory Program was a NASA program of the late 1970s and early 1980s that included a series of three large low Earth orbiting spacecraft for X-ray and Gamma-Ray astronomy and Cosmic-Ray investigations.

[http://en.wikipedia.org/wiki/HEAO\\_Program](http://en.wikipedia.org/wiki/HEAO_Program)

[65] J. J. Engelmann et al., Charge composition and energy spectra of cosmic-ray nuclei for elements from Be to Ni. Results from HEAO-3-C2, *Astron. Astrophys.* 233, 96-111 (1990).

<http://adsabs.harvard.edu/abs/1990A%26A...233...96E>

- [66] C. Zeitlin et al., Overview of the Martian Radiation Environment Experiment (MARIE), *Adv. Spa. Res.* 33, 2204-2210 (2004). [http://dx.doi.org/10.1016/S0273-1177\(03\)00514-3](http://dx.doi.org/10.1016/S0273-1177(03)00514-3)
- [67] C. Zeitlin et al., Mars Odyssey measurements of galactic cosmic rays and solar particles in Mars orbit, 2002–2008, *Space Weather* 8, S00E06 (2010).  
<http://dx.doi.org/10.1029/2009SW000563>
- [68] The goal of the Cosmic Ray Telescope for the Effects of Radiation (CRaTER), one of the Lunar Reconnaissance Orbiter mission instruments, is to characterize the global lunar radiation environment and its biological impacts.. <http://lunar.gsfc.nasa.gov/crater.html>
- [69] H. E. Spence et al., CRaTER: The Cosmic Ray Telescope for the Effects of Radiation Experiment on the Lunar Reconnaissance Orbiter Mission, *Space Sci. Rev.* 150, 243-284 (2010).  
<http://dx.doi.org/10.1007/s11214-009-9584-8>
- [70] A. Posner et al., A high energy telescope for the Solar Orbiter, *Adv. Spa. Res.* 36, 1426-1431 (2005). <http://dx.doi.org/10.1016/j.asr.2004.11.040>
- [71] J. Köhler et al., Inversion of neutron/gamma spectra from scintillator measurements, *Nucl. Instr. and Meth. in Phys. Res., B* 269, 2641-2648 (2011).  
<http://dx.doi.org/10.1016/j.nimb.2011.07.021>
- [72] Nova R & D, Inc., <http://www.novarad.com/products.html>
- [73] A. J. Tylka and W. F. Dietrich, IMP-8 observations of the spectra, composition, and variability of solar heavy ions at high energies relevant to manned space missions, *Radiation Measurements* 30 (1999) 345-359.  
[http://heseweb.nrl.navy.mil/gamma/solar/papers/tylka\\_imp8\\_obs.PDF](http://heseweb.nrl.navy.mil/gamma/solar/papers/tylka_imp8_obs.PDF)
- [74] The Solar Anomalous and Magnetospheric Particle Explorer mission is designed to detect solar energy particles, precipitating energetic electrons, anomalous cosmic rays, and galactic cosmic rays throughout a solar cycle. <http://sunland.gsfc.nasa.gov/smex/sampex/>
- [75] D. N. Baker, G.M. Mason, O. Figueroa, G. Colon, J. G. Watzin, and R. M. Aleman, An Overview of the Solar, Anomalous, and Magnetospheric Particle Explorer (SAMPEX) Mission. *IEEE Trans. Geosci. & Remote Sens.*, 531-541 (1993) <http://dx.doi.org/10.1109/36.225519>

[76] ULYSSES Cosmic and Solar Particle INvestigation (COSPIN) provides measurements of energetic nucleons and electrons in various energy ranges extending upwards from about 0.5 MeV. <http://ulysses.sr.unh.edu/WWW/Simpson/Ulysses.html>

[77] In-situ Measurements of Particles and CME Transients (IMPACT) is a suite of seven instruments that samples the 3-D distribution of solar wind plasma electrons, the characteristics of the solar energetic particle (SEP) ions and electrons, and the local vector magnetic field. <http://sprg.ssl.berkeley.edu/impact/instruments.html>

[78] Ground-based neutron monitors are described in the following article. [http://en.wikipedia.org/wiki/Neutron\\_monitor](http://en.wikipedia.org/wiki/Neutron_monitor)

[79] J. A. Simpson, "The cosmic ray nucleonic component: The invention and scientific uses of the neutron monitor," *Space Sci. Rev.* 93 (1-2), 11–32 (2000). <http://dx.doi.org/10.1023/A:1026567706183>

[80] The University of Delaware's Bartol Research Institute operates a neutron monitoring program. <http://neutronm.bartol.udel.edu/>